

Nonlinear transverse modes of large-aspect-ratio homogeneously broadened lasers:

I. Analysis and numerical simulation

P. K. Jakobsen, J. Lega,* Q. Feng, M. Staley, J. V. Moloney, and A. C. Newell
Arizona Center for Mathematical Sciences, University of Arizona, Tucson, Arizona 85721
 (Received 29 June 1993)

Transverse pattern evolution is investigated in single-longitudinal-mode two-level and Raman lasers with flat end reflectors, subjected to uniform transverse pumping. The natural nonlinear modes of the laser are identified as spatially homogeneous when the detuning from the gain peak is negative and as “local” plane traveling waves when the detuning is positive. The latter correspond to an off-axis emission of the laser. Stability characteristics of the underlying patterns are predicted to be quite different for one-dimensional and two-dimensional (2D) lasers. As an illustration, we provide direct numerical evidence for weakly turbulent behavior of a 2D Raman laser where Eckhaus and zigzag phase instabilities act in concert to spontaneously nucleate topological defects and ridgelike illuminated regions. Our numerics also confirm that the complicated patterns persist for finite transverse pumping as long as the characteristic width of the pump source contains a sufficient number of selected pattern wavelengths.

PACS number(s): 42.55.Px

I. INTRODUCTION

Complex pattern formation is commonly observed in spatially extended, continuous, dissipative systems which are driven far from equilibrium by an external stress. Under the influence of this stress, the system can undergo a series of symmetry-breaking bifurcations or phase transitions and the resulting patterns become more and more complicated, both temporally and spatially, as the stress is increased. Examples abound in ordinary and binary fluids, in liquid crystals and chemically reacting media (for a review, see, for instance, [1] or [2]). Optical systems, both passive and active, are no exception and considerable effort has been expended recently to predict and analyze transverse pattern-forming instabilities in lasers [3–12], parametric oscillators [13], bistable systems [14–32], and counterpropagating waves in Kerr media [33–45]. Experimentally, transverse instabilities have been reported in lasers [46–51], photorefractive oscillators [52], counterpropagating waves in Kerr media [53–59], and liquid crystals [60].

Wide aperture gas and semiconductor lasers offer the possibility of producing high power stable coherent outputs ranging from tens of watts to kilowatts and possibly higher. These lasers also provide ideal physical scenarios for the observation of spatiotemporal complexity in spatially extended dissipative systems. Broad area semiconductor lasers, in particular, are plagued by self-focusing filamentation instabilities and wide aperture gas lasers tend to oscillate in higher order transverse modes of either an induced, or externally imposed, refractive index waveguide. Attempts to produce stabilized coherent outputs has led to the development of nearest neighbor

or globally coupled array geometries [61], although these lasers also tend to oscillate in an out-of-phase mode or undergo complex spatiotemporal pulsations.

In these papers we will illustrate, using the two-level and Raman single-longitudinal-mode lasers as prototype systems, the rich variety of pattern forming instability mechanisms that may appear in wide aperture lasers. We will argue that transverse waveguiding confinement or attempts to impose transverse spatial modes via, say external spherical mirrors, may not represent the optimal approach in efficiently harnessing the lasers output energy. Instead, translational invariance transverse to the laser axis, achieved by uniform pumping and flat end reflectors, allows the gain medium to excite spatially homogeneous or traveling wave modes. We will show that the dynamics of the Maxwell-Bloch laser equations select an exact finite amplitude traveling wave solution for positive detuning ($\Omega > 0$) of the laser and a transverse spatially homogeneous solution for negative detuning ($\Omega < 0$). The traveling wave solution for $\Omega > 0$ manifests itself as an off-axis far-field emission of the laser. A preliminary analysis of these solutions for a two-level laser has already been presented in Ref. [11]. This analysis will be extended further here with an emphasis placed on comparing and contrasting the two-level and the Raman laser models. In particular we will find that it is appropriate to define “local plane wave” transverse modes of the laser which, in contrast to the usual empty resonator modes, are *exact solutions to the full nonlinear laser equations*. Our numerical simulations, while carried out in two transverse space dimensions, show the appearance of a dominant plane traveling wave component irrespective of whether the asymptotic state of the evolution is stationary or weakly turbulent. This traveling wave appears in the far field as an off-axis emission of the laser. A key idea is that in large-aspect-ratio lasers, these solutions of the idealized infinitely extended system, appear as natural states of the laser. One can imagine local patches or domains of transverse patterns

*Permanent address: Institut Non Lineaire de Nice, 1361 Route des Lucioles, 06560 Valbonne, France.

appearing from noise as the laser is turned on. Each local patch separated by domain walls or grain boundaries represents a different state of emission of the laser beam. The possibility then exists for designing innovative injection locking schemes whereby an external probe with an encoded pattern can “lock” a finite region of the laser emission cross section.

In this paper we begin in Sec. II by first introducing the laser models, comparing and contrasting their physical characteristics, and reviewing some elementary bifurcation behavior of the spatially homogeneous solutions. The behavior of the latter is governed by the complex Lorenz equations for the two-level laser and by an interesting extension of these equations for the Raman laser. Our review of the bifurcation behavior of these systems will be necessarily brief, as this has been discussed extensively for the Lorenz equations in both laser [62] and general contexts [63] elsewhere. Some results for the plane wave Raman laser have also appeared recently [64,65]. An interesting observation from the point of view of the present paper is that bifurcation at the first laser threshold is always supercritical for the two-level laser but may be supercritical or nearly subcritical for the Raman laser. As the goal of the present paper is to investigate transverse patterns, we next proceed to carry out a linear stability analysis of both laser systems with transverse degrees of freedom included in Sec. III. By linearizing about the trivial (nonlasing) solution, we note that two cases need to be distinguished: (a) for negative detuning relative to the gain peak (defocusing) the spatially homogeneous state has the lowest threshold whereas, (b) for positive detuning, a transverse traveling wave pattern with selected transverse wave number is excited first. Although the latter solution appears as a spatially uniform near-field intensity distribution, it exhibits an off-axis single-lobed far-field intensity profile at an angle consistent with the selected transverse wave number. The Raman laser adds the interesting additional feature that the effective detuning depends on the magnitude of the stress parameter (external laser pump intensity) due to the presence of a significant ac Stark shift. Emphasis will be placed in Sec. IV on analyzing the finite amplitude lasing traveling wave solutions for the positive detuning case for both laser systems. We identify both phase and amplitude instabilities of the underlying traveling wave in certain ranges of parameter space. Coexistence of stable, Eckhaus [66], Benjamin-Feir [67,68], or zigzag phase instabilities, and amplitude instabilities, at a fixed value of the stress parameter just above the threshold for lasing suggests that extremely rich pattern forming scenarios are possible. The subsequent paper will focus on deriving universal order parameter equations of the complex Ginzburg-Landau or Newell-Whitehead-Segel type, which describe pattern formation in these systems just above threshold and a phase equation which indicates the stability of established patterns well beyond lasing threshold.

Numerical simulations presented in Sec. V confirm that complex pattern evolution is possible just beyond the onset of lasing for both two-level and Raman lasers. The nonlinear detuning due to the ac Stark shift in the Ra-

man laser is seen to significantly extend the pattern forming phenomenology. In particular we provide a specific illustration of the weakly turbulent behavior for a two-dimensional (2D) Raman laser whereby seas of optical vortices [7] (topological defects) and rolllike structures are spontaneously nucleated and transported by the underlying traveling wave. Such complex spatiotemporal behavior can be related to the different phase and amplitude instabilities acting in concert, continually destabilizing the traveling wave. We conclude in Sec. VI with a discussion of the relevance of such patterns, their stability and control to other wide aperture laser systems, such as semiconductor lasers.

II. TWO-LEVEL AND RAMAN LASERS: BACKGROUND THEORY

The essential difference between the two lasers lies in the method of pumping employed in order to achieve population inversion. Figure 1 shows a schematic of the energy level schemes and pumping mechanisms for both lasers. The pump is the principal stress parameter for the problem. Inversion for lasing in a two-level laser is created via incoherent pumping (electrical or flashlamp, rf discharge, collisions, etc.) whereas, in the Raman laser, a classic three-wave interaction involving two optical and one material wave, introduces a strong coherence between the pump wave (amplitude A) and the laser emission field (amplitude e). Figure 1(a) shows incoherent pumping of a broad upper manifold of levels with subsequent decay to form an excess of population in the upper lasing level $|2\rangle$. In the Raman laser depicted in Fig. 1(b), the external pump laser (A) can be detuned either above or below ($\delta < 0$ or > 0) an intermediate dipole coupled level $|2\rangle$ and the laser emission field (e) is generated via the three-wave interaction. Mirror optical feedback in both cases ensures that the finite lasing emission field (e) will build up from noise if the external stress parameter r proportional to the pump in each case exceeds some critical value r_c . The distinction between incoherent and coherent pumping ensures that even the simple plane wave Raman laser should exhibit much richer nonlinear dynamical behavior than its two-level counterpart [64,65].

The mathematical description of both lasers derives di-

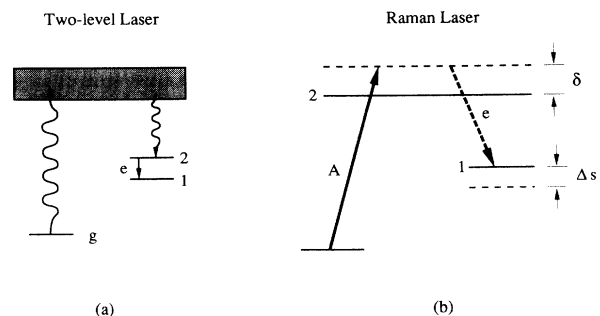


FIG. 1. Energy level diagrams depicting pumping schemes for a (a) two-level and (b) Raman laser.

rectly from the Maxwell equations for the optical fields and the appropriate material density matrix equations. For perfectly flat end reflectors the conventional transverse modes described in terms of Gauss-Laguerre or Hermite-Gaussian functions are frequency degenerate. A key idea is that such modes do not represent the optimum basis for expansion of the laser field. Indeed these mode functions are derived on the assumption of an empty cavity, with the gain medium playing the passive role of supplying photons to the field. Instead we find that the gain medium plays a dominant role in that our “mode” solutions discussed below are exact nonlinear solutions to the laser Maxwell-Bloch (MB) equations. We therefore explicitly include the diffraction operator in the model [4] and write the two-level Maxwell-Bloch equations in the single-longitudinal-mode approximation [69]:

$$\begin{aligned} F_\tau + \kappa F - i \frac{c^2}{2\omega_c w_0^2} \nabla^2 F &= \frac{i\omega_c}{2\epsilon_0} \Lambda, \\ \Lambda_\tau + [\gamma_1 + i(\omega_{12} - \omega_c)] \Lambda &= \frac{i p_{12}^2}{\hbar} F N, \\ N_\tau + \gamma_2 (N - N_0) &= \frac{2i}{\hbar} (F^* \Lambda - F \Lambda^*), \end{aligned}$$

where F and Λ are the envelope variables of the electric and polarization fields, κ is the cavity damping coefficient, c is the speed of light in vacuum, ω_c is the frequency of the single longitudinal mode, w_0 is the beam waist, ϵ_0 is the vacuum permittivity, γ_1 is the dipole dephasing rate, ω_{12} is the two-level atom transition frequency, p_{12} is the dipole matrix element coupling the two levels, N is the atomic inversion, N_0 is the initial inversion, γ_2 is the inversion decay rate, and \hbar is Planck’s constant. It is convenient to make the following changes of variables:

$$\begin{aligned} \tau &= \frac{t}{\gamma_1}, & F &= \frac{i\hbar\gamma_1}{2p_{12}} e, \\ \Lambda &= \frac{\hbar\gamma_1\epsilon_0\kappa}{\omega_c p_{12}} p & N - N_0 &= \frac{2\epsilon_0\kappa\hbar\gamma_1}{\omega_c p_{12}^2} n, \end{aligned}$$

and write the Maxwell-Bloch equation in complex Lorenz notation:

$$\begin{aligned} e_t - ia \nabla^2 e &= -\sigma e + \sigma p, \\ p_t + (1 + i\Omega)p &= (r - n)e + i\delta_2 |e|^2 p, \\ n_t + bn &= \frac{1}{2}(e^* p + ep^*), \end{aligned} \quad (1)$$

where

$$\begin{aligned} \sigma &= \frac{\kappa}{\gamma_1}, & \Omega &= \frac{\omega_{12} - \omega_c}{\gamma_1}, & b &= \frac{\gamma_2}{\gamma_1}, \\ r &= \frac{\omega_c p_{12}^2 |N_0|}{2\epsilon_0 \hbar \kappa \gamma_1}, & a &= \frac{c^2}{2\omega_c w_0^2 \gamma_1}. \end{aligned}$$

The model for the Raman laser is an extension of the plane wave model given in Refs. [64,65] to include diffraction and when scaled using complex Lorenz notation (see the Appendix) takes the form

$$\begin{aligned} e_t - ia \nabla^2 e &= -\sigma e + \sigma p + i\delta_1 en, \\ p_t + (1 + i\Omega)p &= (r - n)e + i\delta_2 |e|^2 p, \\ n_t + bn &= \frac{1}{2}(e^* p + ep^*), \end{aligned} \quad (2)$$

with $\Omega = (\omega_{12} - \omega_c)/\gamma_1 + r\delta_3$.

The essential difference between the Raman and two-level laser lies in the presence of a nonlinear detuning term in the former. This term arises from the ac Stark shift and appears in the definition of Ω as an adjustment to the passive frequency due to the presence of an external pump and as an active intensity dependent detuning through the term proportional to δ_2 . The scaling from the original notation used in Refs. [64,65] to complex Lorenz notation is outlined in the Appendix. The stress parameter r now depends on the external pump laser intensity A^2 , $r = \frac{A^2 |N_0| g}{\delta^2 \gamma_1^2 \sigma}$ ($N_0 < 0$), with δ representing the detuning of the pump laser from the dipole coupled off-resonant intermediate state 2 (see Fig. 1). The coefficients δ_i , $i = 1, 2, 3$, are defined in the Appendix. When these are set to zero we recover the form of the two-level complex Lorenz equations (1).

The plane wave (spatially homogeneous in x and y) solutions to Eqs. (1) and (2) will form the starting point for the analysis of transverse patterns. Both laser models admit a trivial (nonlasing) solution $(e, p, n) = (0, 0, 0)$. Importantly, both laser models admit an exact traveling wave solution $(e, p, n) = [\bar{e}e^{i\theta}, \bar{p}e^{i\theta}, \bar{n}]$. Note in particular that the standing wave $(e, p, n) = [\bar{e}e^{i\theta} + \cdot, \bar{p}e^{i\theta} + \cdot, \bar{n}]$ is *not an exact solution*. We showed in a previous publication [11] that the traveling wave solution appeared to be globally attracting for a 1D two-level laser when $\Omega > 0$. In a large aspect ratio system ($a \ll 1$) we anticipate that these traveling waves will act as the natural nonlinear “local plane wave” modes of the laser due to the fact that transverse boundaries are remote.

III. LINEAR STABILITY ANALYSIS OF NONLASING SOLUTION

Linearization about the trivial (nonlasing) solution yields the laser frequency shift and critical stress parameter at onset of lasing [69],

$$\nu_c = \frac{\sigma\Omega_c + ak^2}{\sigma + 1} \quad r_c = 1 + \frac{(\Omega_c - ak^2)^2}{(\sigma + 1)^2}, \quad (3)$$

where $\Omega_c = (\omega_{12} - \omega_c)/\gamma_1$ for the two-level and $\Omega_c = (\omega_{12} - \omega_c)/\gamma_1 + r_c\delta_3$ for the Raman laser is the value of Ω at threshold. The formula for the laser oscillation frequency

$$\begin{aligned} \omega_L &= \omega_c + \gamma_1 \nu_c \\ &= (\omega_c + \sigma(\omega_{12} + r\gamma_1\delta_3) + \gamma_1 ak^2)/(\sigma + 1) \end{aligned}$$

is a simple generalization of the classical frequency pulling formula for a laser (the $r\gamma_1\delta_3$ term is missing for the two-level laser). For Ω positive we then have the simple physical picture that the laser will seek to develop

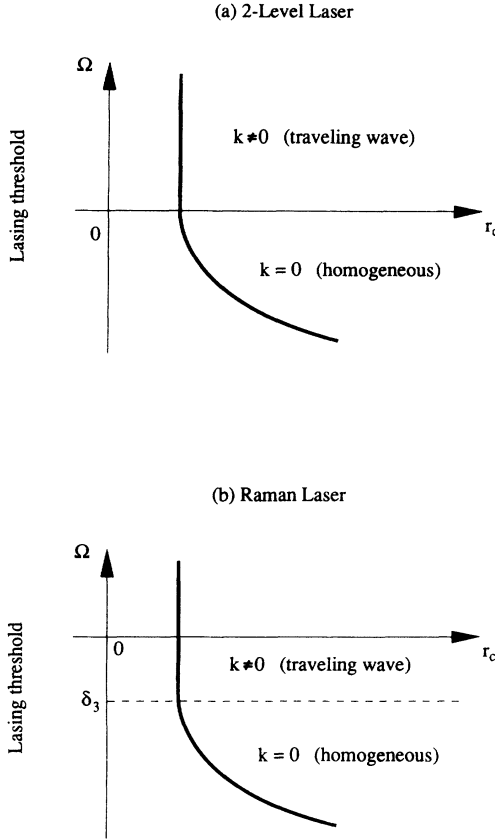


FIG. 2. Stability and instability regions for the nonlasing solution in (Ω, r_c) parameter space. (a) Two-level and (b) Raman laser.

a transverse laser pattern with wave number $k_0 = \sqrt{\frac{\Omega_c}{a}}$, which minimizes the detuning, thereby maximizing the gain. Furthermore for $\Omega < 0$, the spatially homogeneous state ($k = 0$) has the lowest threshold with $r_c = 1 + \frac{\Omega_c^2}{(\sigma+1)^2}$ whereas, for $\Omega > 0$, the mode with $k_0 = \sqrt{\frac{\Omega_c}{a}}$ has the lowest threshold at $r_c = 1$. The stability characteristics of the nonlasing solution are succinctly captured in the (Ω, r_c) plane in Fig. 2 for both lasers. Increasing the stress parameter r in Fig. 2(a) at a fixed detuning Ω corresponds to moving horizontally to the right in this figure. Because of the dependence of the frequency Ω on stress parameter r for the Raman laser, increasing r at a fixed detuning corresponds to moving on a curve in the

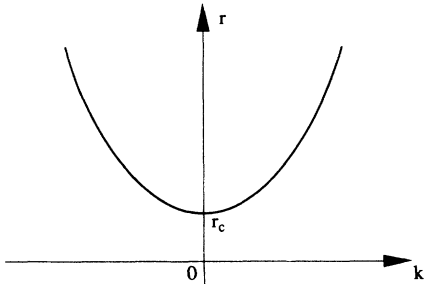


FIG. 3. Sketch of the neutral stability curve for $\Omega < 0$. The homogeneous state ($k_0 = 0$) has the lowest threshold.

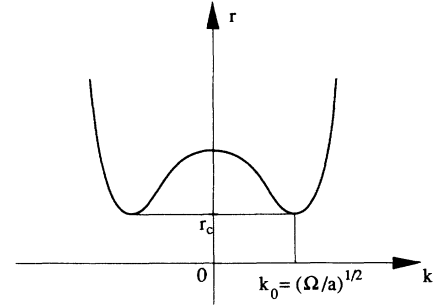


FIG. 4. Sketch of the neutral stability curve for $\Omega > 0$. The homogeneous state ($k_0 = \sqrt{\Omega_c/a}$) has the lowest threshold.

(Ω, r_c) plane.

Different spatiotemporal transverse structures may be expected to emerge when the laser passes through threshold for $\Omega > 0$ and $\Omega < 0$. A graph of the neutral stability curve $[r(k) \text{ vs } k]$ for both signs of the detuning is shown in Figs. 3 and 4. For $\Omega < 0$ a finite band of transverse wave numbers (in x and y) centered on $|k| = 0$ can be excited. This case has been discussed in Ref. [7] for a two-level laser. On the positive detuning side ($\Omega > 0$), two continuous bands of active modes can be excited leading to the expectation that a standing wave pattern with wave number $k_0 = \pm\sqrt{\Omega/a}$ should be excited. We will see, however, through numerics in this paper and through weakly nonlinear analysis in the following paper that the traveling wave state (at either $+k_0$ or $-k_0$) is favored. This traveling wave solution is given explicitly in the next section.

IV. BEYOND LASER THRESHOLD: STABILITY OF TRAVELING WAVE

When $r > r_c$, the two-level laser undergoes a supercritical (Hopf) bifurcation to a spatially homogeneous lasing state for $\Omega < 0$ or to a traveling wave state $(e, p, n) = (\bar{e}e^{i\theta}, \bar{p}e^{i\theta}, \bar{n})$, $\theta = \mathbf{k} \cdot \mathbf{x} + \omega t$ for $\Omega > 0$ with

$$\begin{aligned} \bar{e}^2 &= \frac{b}{(1+\sigma)^2} [(r-1)(1+\sigma)^2 - a^2(k^2 - k_c^2)^2], \\ \bar{p} &= \left(1 + \frac{i}{\sigma}(\omega + ak^2)\right) \bar{e}, \\ \bar{n} &= \frac{\bar{e}^2}{b}, \end{aligned} \quad (4)$$

and $\omega = -\frac{1}{(\sigma+1)}(\sigma\Omega + ak^2)$. In the Raman laser a similar transition to a homogeneous ($\Omega < 0$) or traveling wave ($\Omega > 0$) state is observed, although in this case the bifurcation to the latter may be sub- or supercritical. The lasing emission intensity \bar{e}^2 (can be assumed real) is now given as the solution to the following quadratic equation in \bar{e}^2 :

$$\begin{aligned} \left(\frac{\delta_1}{b} - \delta_2\right)^2 \bar{e}^4 + \left[2(\Omega - ak^2) \left(\frac{\delta_1}{b} - \delta_2\right) + \frac{(1+\sigma)^2}{b}\right] \bar{e}^2 \\ + (\Omega - ak^2)^2 - (r-1)(1+\sigma)^2 = 0 \end{aligned} \quad (5)$$

with $\omega = \frac{1}{\sigma+1}[\sigma\delta_2\bar{e}^2 - \sigma\Omega - ak^2 + \delta_1\bar{e}^2/b]$, $\bar{n} = \bar{e}^2/b$, $\bar{p} = \bar{e}(1 + i\alpha)$, and $\alpha = \frac{1}{(\sigma+1)}[\bar{e}^2(\delta_2 - \frac{\delta_1}{b}) - (\Omega - ak^2)]$.

It is shown in the Appendix that the bifurcation to this state will be subcritical if the condition $[2(\Omega - ak^2)(\frac{\delta_1}{b} - \delta_2) + \frac{(\sigma+1)^2}{b}] < 0$ is satisfied.

The neutral stability curve in Fig. 4 shows the existence domain for traveling waves as a function of transverse spatial wave number k . We next explore the stability of these traveling wave solutions to finite sideband perturbations by linearizing about the basic traveling wave solution given by Eqs. (4) for a two-level laser, or (5) for a Raman laser. Setting

$$\begin{aligned} e &= (\bar{e} + e_1 e^{i\mathbf{h}\cdot\mathbf{x}} + \tilde{e}_1 e^{-i\mathbf{h}\cdot\mathbf{x}}) e^{i\theta}, \\ p &= (\bar{p} + p_1 e^{i\mathbf{h}\cdot\mathbf{x}} + \tilde{p}_1 e^{-i\mathbf{h}\cdot\mathbf{x}}) e^{i\theta}, \\ n &= \bar{n} + n_1 e^{i\mathbf{h}\cdot\mathbf{x}} + \tilde{n}_1 e^{-i\mathbf{h}\cdot\mathbf{x}}, \end{aligned} \quad (6)$$

where \mathbf{h} is the perturbation wave vector, we obtain the growth rates for sideband perturbations, parametrized by the traveling wave number k , for regions above the neutral stability curve in Fig. 4. Note that we must assume a fixed direction for the underlying traveling wave and consider perturbations at arbitrary directions relative to this fixed direction for the 2D (x - y) case.

The translational symmetry of the problem ensures the existence of a neutral mode (eigenvalue with vanishing real part) at $h = 0$ and we identify long wavelength unstable growth bands emanating from this neutrally stable point as phase instabilities. Amplitude instabilities occur at shorter wavelengths and correspond to modes which are not neutral at $h = 0$. This distinction becomes especially important in the next paper when we derive a phase equation which will account for such phase instabilities but not for amplitude ones. Of course, the amplitude equations to be derived in the next paper account for both types of instability, but these are strictly valid close to threshold. The phase equation, on the other hand, will be seen to give an accurate description of phase instabilities both near and well above laser threshold. Figure 5 provides a succinct summary of the types of instability found for the full MB laser equations under consideration here. Of the phase instabilities, the Eckhaus [66] is the most common 1D instability, occurring along the direction of the traveling wave. This instability is often responsible for the spontaneous introduction of topological defects in stable patterns by causing a local modification of the pattern wavenumber [70,71]. The Benjamin-Feir [67,68] or modulational instability is less common, at least for the nonstiff limit of the laser equations dealt with here. By nonstiff limit we refer to the case where all damping coefficients in the Maxwell-Bloch equations have comparable magnitudes. The zigzag phase instability occurring at right angles to the traveling wave direction is the only 2D phase instability found to date in lasers. We anticipate therefore that the nature of pattern formation and dynamics will be fundamentally different for 1D and 2D wide aperture lasers as the zigzag instability is obviously absent in the former. A variety of amplitude instabilities have been found in 1D both near and well beyond lasing threshold. The situation is sufficiently complex even in 1D that we put off a detailed analysis of these instabilities to a future paper. Detailed

CLASSIFICATION OF PATTERN FORMING INSTABILITIES

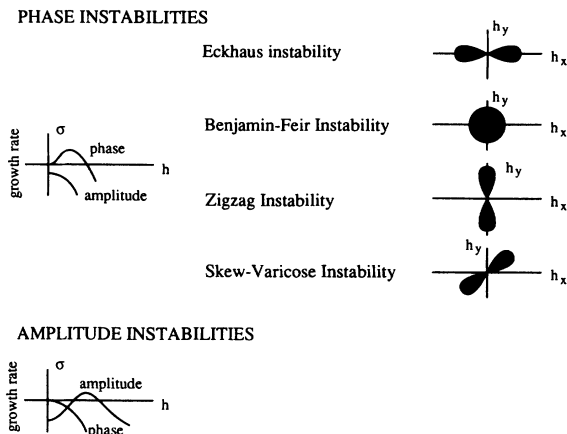


FIG. 5. Typical phase and amplitude instabilities of an underlying traveling wave expected for two-level and Raman lasers. The traveling wave direction is assumed to be along the x axis.

numerical simulations will be presented in Sec. V for the 2D Raman laser in a situation where such instabilities are known to be absent.

As an illustration, we now fill in the phase and amplitude instability boundaries above the neutral stability curve for the case of a two-level laser with parameters given in the figure caption. The symmetry of the picture allows us to show details only for the right half (positive k) of the neutral curve plot. The vertical dash-dotted line in Fig. 6 represents the maximum emission state of the laser given by $k_0 = \sqrt{\frac{\Omega}{a}}$. Our earlier numerical studies of the 1D two-level laser indicate that this appears to be a globally attracting solution [11]. Eckhaus unstable bands straddle a wide region of stable traveling wave solutions; the latter we refer to as the Busse balloon, [72] consistent with fluid dynamics terminology. A zig-zag (2D) unstable band lies to the immediate left of the maximum emission solution at $k = k_0$ and extends all of the way to the left boundary out to the neutral stability curve.

The Raman laser at similar parameter values shows some additional features to the two-level laser. The external pump laser may be tuned above or below the intermediate nonresonant dipole coupled level. The case where the pump is tuned below the intermediate level exhibits the closest resemblance to the two-level case with the large stable traveling wave region (Busse balloon) extending all of the way down to threshold. This case is shown in Fig. 7. The dependence of the maximum emission state of the laser on external pump intensity (stress parameter τ) is evident from the curvature of the dash-dotted line representing this solution in the figure. The lower left-hand dashed curve delimits the region of existence of traveling waves. It is in general identical to the neutral stability curve. When it departs from this latter curve, the bifurcation is subcritical at the corresponding wave vector k . Between these two curves the

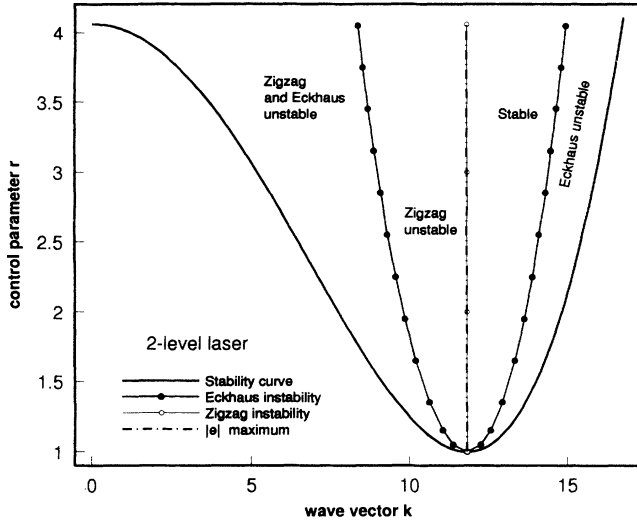


FIG. 6. Neutral stability curve and phase instability boundaries as computed from the phase equation for the two-level laser. The parameters used are $a = 0.05$, $\sigma = 3.00$, $\Omega = 7.00$, and $b = 0.83$.

stable nonlasing state and stable or unstable finite amplitude laser emission state coexist within a finite parameter window. The zigzag unstable band now crosses the maximum emission state curve into the Busse balloon. In the two-level laser the right-hand boundary of the zigzag unstable band was determined by $k_0 = \sqrt{\frac{\Omega}{a}}$ (see Fig. 6).

By simply tuning the external laser above the intermediate level we can modify this stability picture significantly. Figure 8 illustrates this change in stability characteristics. Parameters used to generate this figure are given in the caption of Fig. 7; the sign of the intermediate detuning is simply reversed. The stable (Busse

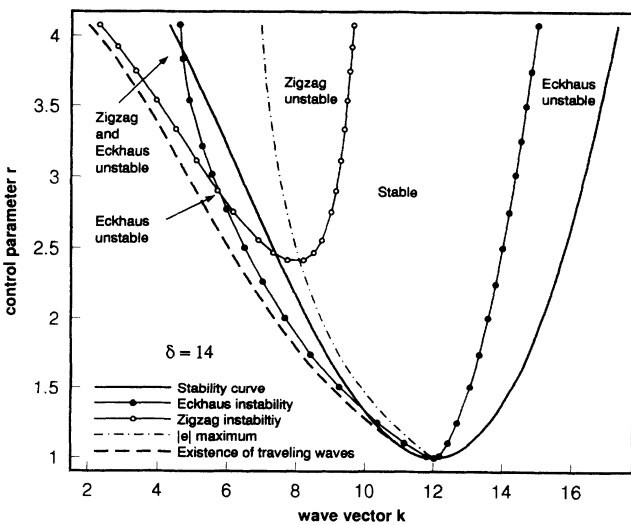


FIG. 7. Neutral stability curve and phase instability boundaries as computed from the phase equation for the Raman laser. The parameters used are the same as in Fig. 6, with $\sigma = 3.00$, $\gamma_1 = 1.00$, $\gamma_2 = 0.83$, $g = 180.00$, $\Delta_s = -7.00$, $\rho = 1$, and $\delta = 14$.

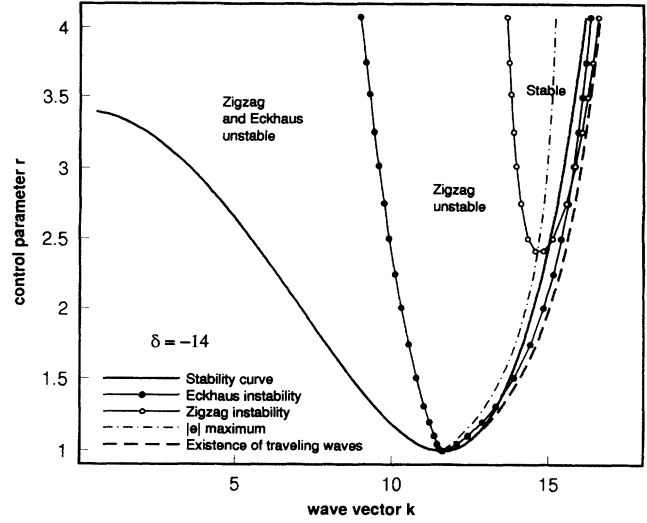


FIG. 8. Same as Fig. 7, but for $\delta = -14$.

balloon) region is now moved well above the laser threshold, the disposition of the maximum emission state curve and subcritical bifurcation curve are changed relative to Fig. 7, and the zigzag unstable region now extends down to lasing threshold. There now exists a substantial domain immediately above lasing threshold where no stable output of the laser exists. We will use this picture to illustrate some 2D numerical simulations in the next section which show weakly turbulent behavior.

Figure 9 gives an example where the traveling wave is Benjamin-Feir unstable right above threshold. In this case, there is no k for which the traveling wave solution is stable near threshold, even in one dimension.

It is evident from a scan of this limited span of physical parameter space that wide aperture two-level and Raman lasers should exhibit extremely rich and varied pattern forming instabilities. The above analysis assumes an infinitely extended transverse dimension and the question naturally arises as to how finite boundaries may modify such predictions. We confirm in the next section that

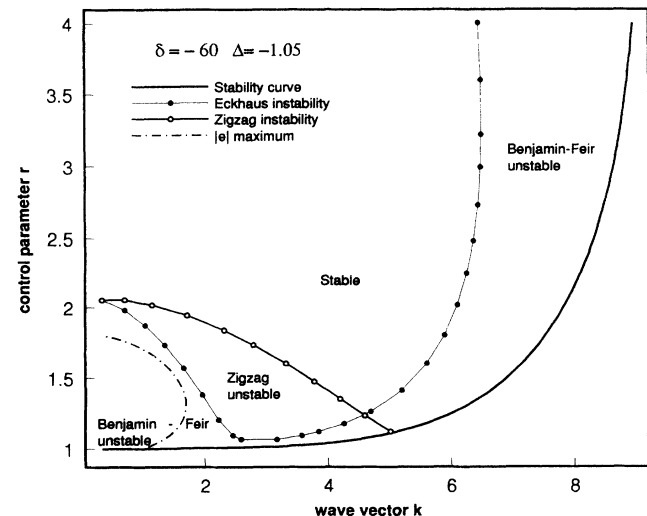


FIG. 9. Same as Fig. 7, but for $\delta = -60$ and $\Delta_s = -1.05$.

if the aspect ratio of the laser is sufficiently large to incorporate a finite number of wave numbers k within any boundaries, we may expect many features of this idealized infinitely extended model to persist.

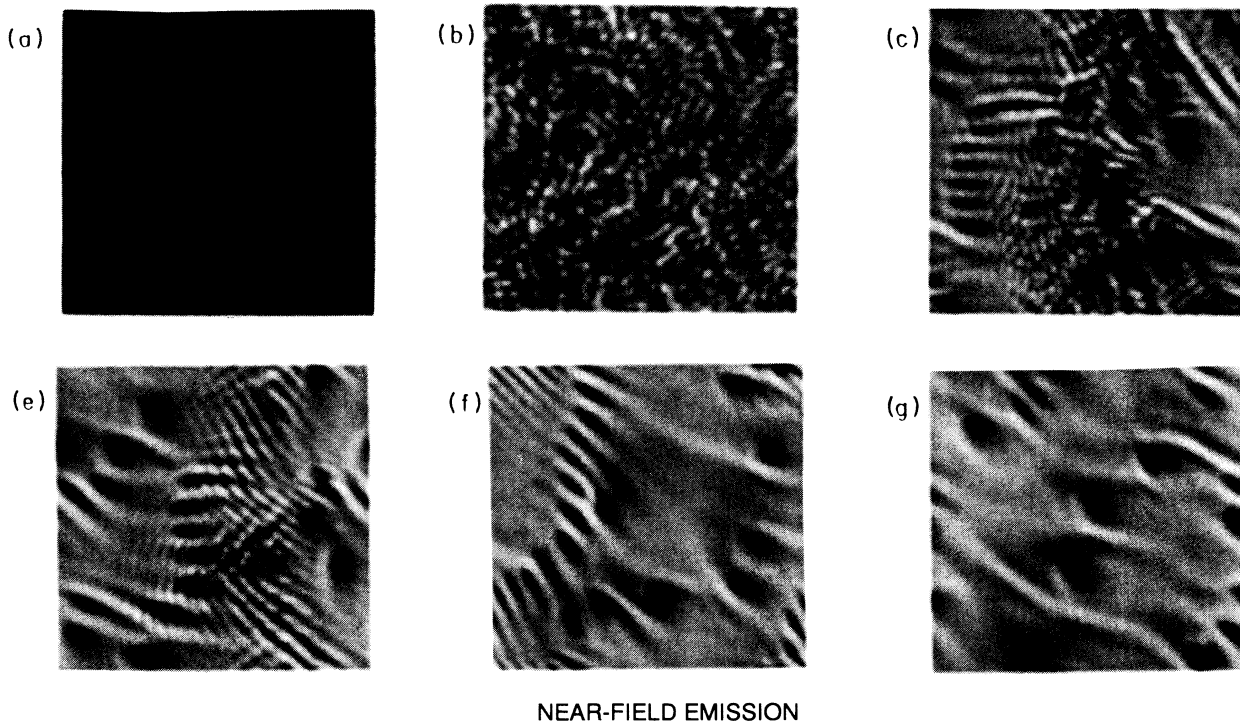
V. NUMERICAL SIMULATIONS

We now use Fig. 8 to illustrate how patterns may develop across the laser crosssection, when the stress parameter r is chosen so that Eckhaus, zigzag unstable, and stable traveling wave solutions coexist. The Maxwell-Bloch equations have been numerically integrated using a split-step spectral algorithm. The numerical procedure was used to confirm that the traveling wave solution (5) with wave number k selected so as to lie within the Busse balloon, remained asymptotically stable. Figures 10 and 11 show a sequence of frames from a movie of the near- and far-field x - y output cross sections of a Raman laser, when the pump is chosen so that the Eckhaus, zigzag unstable, and stable Busse balloon coexist. The field is initiated from noise and the near-field pictures show the buildup from noise (random pattern) to a finite amplitude emission consisting of a sea of optical vortices [7] (zeros of the complex field) and bright ridges which arise from a combination of Eckhaus and zigzag instabilities. The bright ridges are alligned at right angles to the local direction of the traveling wave which moves from the top right to bottom left corner in these frames. Frame (a) shows the noisy transverse spatial pattern which has grown from the initial noise seed. As the pattern grows in

amplitude, some semblance of regularity begins to appear initially on small scales [frames (b) and (c)]. Eventually, large-scale transverse structures appear superimposed on the uniform plane transverse traveling wave background [see frames (d) and (e)]. Although the system never settles into a quiescent state, the final frame (f) is indicative of the weakly turbulent behavior which persists. This complicated spatiotemporal evolution appears to persist indefinitely with no sign of any regular recurrence.

The far-field emission shows the appearance of a weak ring in Fourier (k_x, k_y) space [Fig. 11(a)] whose radius initially corresponds to the value $k = k_c$ at threshold. This reflects the fact that there is initially no preferred direction in space. As the amplitude of the noisy state grows, the ring expands slightly [frame (b)], consistent with the fact that the critical wave number depends on intensity for the Raman laser. This degeneracy is broken in frames (c) and (d) once the amplitude grows and a direction is established. The far-field emission remains off axis, appearing as an intense fairly localized spot [frames (e) and (f)]. This spot tends to shift back and forth in a random fashion while maintaining a lower amplitude fluctuating background, indicative of a weakly turbulent state of the laser emission.

We have also tested the robustness of the plane traveling wave solution to different perturbations by injecting different external patterns via a weak external probe beam. The degeneracy in wave number selection as exemplified by the annular band of excited modes in wave number space, might suggest that a wide range of patterns may be excited. Probe beams were injected so as to



NEAR-FIELD EMISSION

FIG. 10. Six frames from a movie showing the near-field (x, y) outputs of a Raman laser when the stress parameter $r = 3$. The other parameters are those of Fig. 8.

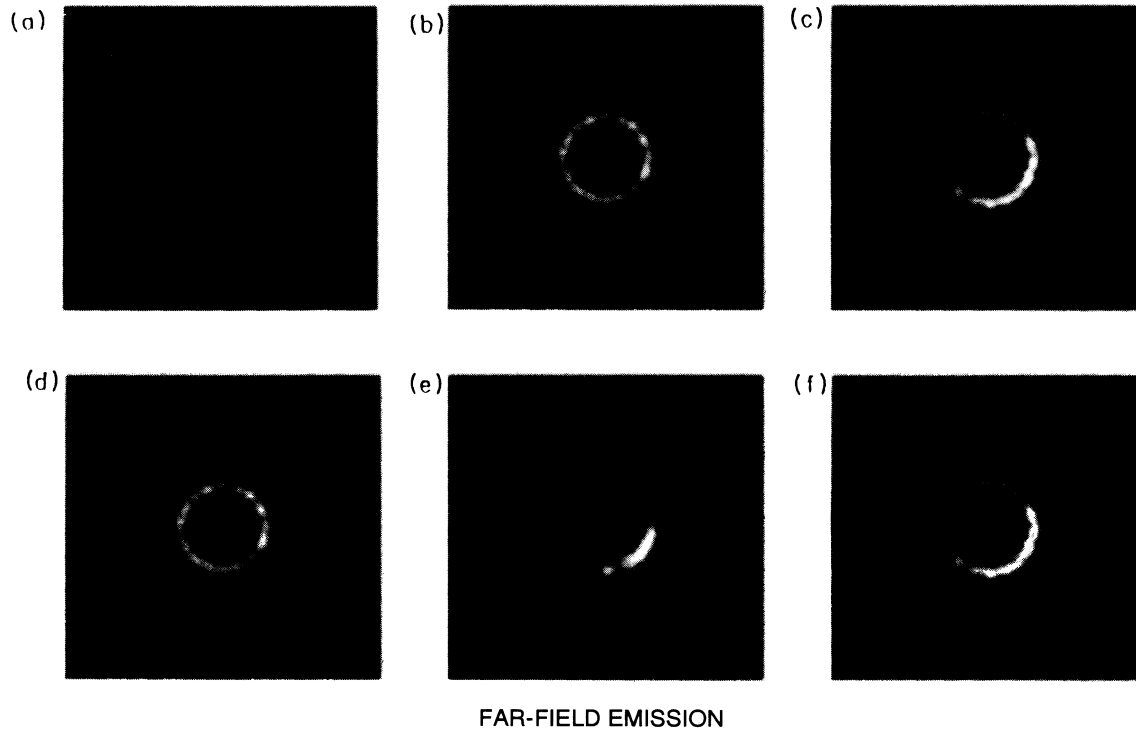


FIG. 11. Same as Fig. 10 for the corresponding far-field (k_x , k_y) outputs.

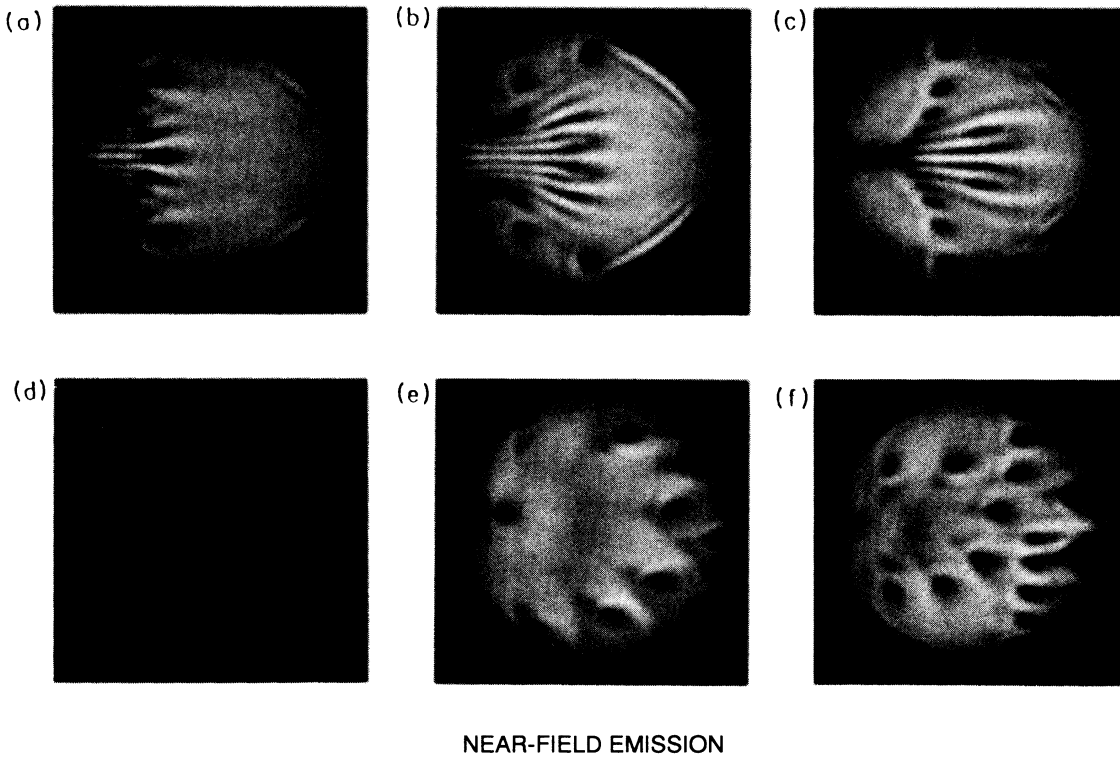


FIG. 12. Near-field outputs of a Raman laser for a super-Gaussian pump, with an effective $r = 4$. The other parameters are those of Fig. 8.

lie within the annulus and a two and hexagonal spot pattern were excited. These persisted as long as the probe beams remained on. Once the injected beams were removed, the pattern quickly degenerated to a pulsating single far-field off-axis spot. When the probe is injected so as to excite the zigzag instability at right angles to the traveling wave with the most unstable wave number for this instability as a seed, we observe the growth of a spatially modulated pattern at right angles to the traveling wave direction. This grows into a saturated solitary wave train. Figure 12 shows that the same qualitative spatiotemporal features persist even when the transverse pumping domain is finite. This shows a series of six frames of the laser output for a super-Gaussian pump where the outer dark region is strongly absorbing. The pump parameter $r(x, y)$ is assumed to have a flat topped shape with a rapid falloff at the edges. The traveling wave and weakly turbulent patterns persist when the aspect ratio of the laser is large enough.

VI. CONCLUSIONS

Both two-level and Raman wide aperture lasers are capable of displaying a rich variety of pattern forming instabilities. The nonlinear detuning term in the Raman laser is responsible for promoting a broader range of instability behavior than can occur in the two-level laser. The nature of the instability depends on the transverse dimension of the laser system and it is anticipated that much of the spatiotemporal behavior of these lasers will carry over to technologically important wide aperture semiconductor laser systems. The latter systems require a much more complicated material description, involving many-body interactions between carriers and holes at the microscopic level and a major challenge that remains is to derive order parameter equations near onset that are capable of predicting and suggesting means of stabilization of novel pattern shapes in broad area and vertical cavity surface emitting semiconductor lasers.

ACKNOWLEDGMENTS

The authors wish to thank the Arizona Center for Mathematical Sciences (ACMS) for support. ACMS is sponsored by AFOSR Contract No. F49620-94-1-0144DEF. Two of the authors (J.V.M. and J.L.) acknowledge partial support for this work from a European Community Twinning Grant No. SCI*0325-C(SMA).

APPENDIX: BASIC PROPERTIES OF SIMPLE SOLUTIONS TO THE RAMAN LASER MODEL

The three coupled partial differential equations that model a Raman laser [64,65] are

$$\begin{aligned} E_{t'} + \mu E - i\hat{a}\nabla^2 E &= -\frac{g}{\delta}AP - i\frac{g}{2\delta}E(N - N_0), \\ P_{t'} + \gamma_1(1 + i\Omega)P &= \frac{1}{\delta}AEN_0 + \frac{1}{\delta}AE(N - N_0) \\ &\quad + i\gamma_1\frac{\rho}{\delta}|E|^2P, \\ N_{t'} + \gamma_2(N - N_0) &= -\frac{2}{\delta}A(E^*P + EP^*), \end{aligned}$$

where the electric field E and the polarization P are complex quantities, and the population inversion N is real. In the following, we use dimensionless equations:

$$\begin{aligned} e_t - ia\nabla^2 e &= -\sigma e + \sigma p + i\delta_1 en, \\ p_t + (1 + i\Omega)p &= (r - n)e + i\delta_2 |e|^2 p, \\ n_t + bn &= \frac{1}{2}(e^*p + ep^*), \end{aligned} \quad (\text{A1})$$

where

$$\begin{aligned} a &= \frac{\hat{a}}{\gamma_1}, \quad t = \gamma_1 t', \\ e &= \frac{2A}{\delta\gamma_1}E, \quad p = -\frac{2gA^2}{\delta^2\mu\gamma_1}P, \quad n = \frac{gA^2}{\delta^2\mu\gamma_1}(N - N_0), \\ \sigma &= \frac{\mu}{\gamma_1}, \quad b = \frac{\gamma_2}{\gamma_1}, \quad r = \frac{A^2|N_0|g}{\delta^2\gamma_1^2\sigma} \quad (N_0 < 0), \\ \delta_1 &= -\frac{\mu\delta}{2A^2}, \quad \delta_2 = \frac{\rho\delta\gamma_1^2}{4A^2}, \\ \Omega &= -\Delta_s + \frac{\rho}{\delta}A^2 = \Delta + \frac{\rho}{\delta}A^2. \end{aligned}$$

1. Stability of the nonlasing state

The rest state is given by $e = 0$, $p = 0$, and $n = 0$. The linearized system obtained from (A1) linearized about $(e = 0, p = 0, n = 0)$ is

$$\begin{aligned} e_t &= (-\sigma - iah^2)e + \sigma p, \\ p_t &= -(1 + i\Omega)p + re, \\ n_t &= -bn, \end{aligned}$$

where h is the wave vector of the perturbation. The corresponding eigenvalues are then

$$\begin{aligned} \lambda_n &= -b, \\ \lambda_{\pm} &= -\frac{1 + i\Omega + \sigma + iah^2}{2} \pm (\alpha + i\beta), \end{aligned}$$

where

$$\alpha + i\beta = \sqrt{\left(\frac{1 + i\Omega - iah^2 - \sigma}{2}\right)^2 + \sigma r}, \quad \alpha > 0. \quad (\text{A2})$$

The nonlasing state becomes unstable when one of the eigenvalues has a positive real part, i.e., when

$$\alpha^2 > \left(\frac{1 + \sigma}{2}\right)^2.$$

Using (A2), we find that α^2 is solution to $P(\alpha^2) = 0$ where P is a polynomial of degree 2:

$$P(\alpha^2) = \alpha^4 - \left(\frac{(1-\sigma)^2 - (\Omega - ah^2)^2}{4} + \sigma r \right) \alpha^2 - \frac{1}{16} (1-\sigma)^2 (\Omega - ah^2)^2.$$

The condition $\alpha^2 > [(1+\sigma)/2]^2$ is then equivalent to $P\{[(1+\sigma)/2]^2\} < 0$. Since

$$P\left[\left(\frac{1+\sigma}{2}\right)^2\right] = \frac{\sigma}{4} [(1+\sigma)^2(1-r) + (\Omega - ah^2)^2],$$

the neutral stability curve is given by

$$(1+\sigma)^2(1-r) + (\Omega - ah^2)^2 < 0,$$

i.e.,

$$G(r, h^2) = (1+\sigma)^2(1-r) + (-\Delta_s - ah^2 + r\delta_3)^2 < 0,$$

where

$$\delta_3 = \frac{\rho\delta\mu\gamma_1}{g|N_0|}.$$

For each h , we need to find the value(s) of r for which the nonlasing state becomes unstable. The smallest value of r will give the instability threshold and the critical wavevector. G is minimal for

$$h_{\min}^2 = \frac{1}{a}(r\delta_3 - \Delta_s).$$

Two situations can occur.

If $1/r > r_0 = \frac{\Delta_s}{\delta_3}$, then

$$G_{\min}(r) = G(r, h_{\min}^2) = (1+\sigma)^2(1-r).$$

If $2/r < r_0 = \frac{\Delta_s}{\delta_3}$, then

$$G_{\min}(r) = G(r, 0) = (1+\sigma)^2(1-r) + (r\delta_3 - \Delta_s)^2 = (1+\sigma)^2(1-r) + \delta_3^2(r - r_0)^2.$$

If $r_0 > 1$, G_{\min} vanishes at $r = r_c$ where $r_c > 1$ and r_c is solution to $(1+\sigma)^2(1-r_c) + \delta_3^2(r_c - r_0)^2 = 0$. The critical wave vector is then $h_c = 0$. With $\Omega_c = -\Delta_s + r_c\delta_3$, we get $\Omega_c < 0$ and $(1+\sigma)^2(1-r_c) + \Omega_c^2 = 0$ i.e., $r_c = 1 + \frac{\Omega_c^2}{(1+\sigma)^2}$. The imaginary part of the eigenvalue λ_+ whose real part vanishes at threshold is then $-\nu_c = -\sigma\Omega_c/(1+\sigma)$.

If $r_0 < 1$, G_{\min} vanishes for $r_c = 1$ and $h_c^2 = \frac{\delta_3 - \Delta_s}{a} = \frac{\Omega_c}{a}$. The frequency of the Hopf bifurcation is then $-\nu_c = -(\Omega_c + ah_c^2)/2$.

In the plane (Ω, r_c) , the critical curve is made of part of the straight line $r_c = 1$ and of a piece of the parabola $r_c = 1 + \Omega_c^2/(1+\sigma)^2$ (see Fig. 2). The two formulas for ν_c can be condensed in

$$\nu_c = \frac{\sigma\Omega_c + ah_c^2}{1+\sigma}.$$

2. Solutions above threshold

We assume $\Delta_s > \delta_3$, i.e., $r_c = 1$ and $h_c^2 = \frac{\Omega_c}{a}$. Above threshold, system (A1) admits traveling wave solutions

of the form

$$e = \bar{e}e^{i(\mathbf{h}\cdot\mathbf{r} + \omega t)}, \quad p = \bar{p}e^{i(\mathbf{h}\cdot\mathbf{r} + \omega t)}, \quad n = \bar{n},$$

where \bar{e} and \bar{n} are real numbers whereas \bar{p} is a complex quantity. The amplitude \bar{e} of the electric field is solution to the following equation:

$$\left(\frac{\delta_1}{b} - \delta_2\right)^2 \bar{e}^4 + \left[2(\Omega - ah^2) \left(\frac{\delta_1}{b} - \delta_2\right) + \frac{(1+\sigma)^2}{b}\right] \bar{e}^2 + (\Omega - ah^2)^2 - (r-1)(1+\sigma)^2 = 0, \quad (\text{A3})$$

where

$$\omega = \frac{1}{1+\sigma} \left[\sigma\delta_2\bar{e}^2 - \sigma\Omega - ah^2 + \delta_1\frac{\bar{e}^2}{b} \right],$$

$$n = \frac{\bar{e}^2}{b},$$

$$\bar{p} = \bar{e}(1+i\alpha),$$

$$\alpha = \frac{1}{\sigma}(\omega + ah^2 - \delta_1 n)$$

$$= \frac{1}{1+\sigma} \left[\bar{e}^2 \left(\delta_2 - \frac{\delta_1}{b} \right) - (\Omega - ah^2) \right].$$

3. Nature of the bifurcation

The product of the two roots of (A3) (taken as a polynomial of degree 2 in \bar{e}^2) is equal to

$$\left(\frac{\delta_1}{b} - \delta_2\right)^{-2} [(\Omega - ah^2)^2 - (r-1)(1+\sigma)^2] = \left(\frac{\delta_1}{b} - \delta_2\right)^{-2} G(r, h^2)$$

and is always negative above threshold. However, at threshold, one root is zero and the other one is equal to the sum of the roots of (A3), i.e., to

$$-\left(\frac{\delta_1}{b} - \delta_2\right)^{-2} \left[2(\Omega - ah^2) \left(\frac{\delta_1}{b} - \delta_2\right) + \frac{(1+\sigma)^2}{b} \right].$$

If this other root is positive, the bifurcation is subcritical for some values of h since the system then admits non-zero solutions below threshold. On the neutral curve, the product of the two roots is equal to zero, i.e.,

$$\Omega - ah^2 = \varepsilon\sqrt{r-1}(1+\sigma),$$

where $\varepsilon = \pm 1$. With

$$\delta_1 - b\delta_2 = -\frac{\sigma\delta}{2A^2} - \frac{\rho b\delta\gamma_1^2}{4A^2} = -\delta\frac{|N_0|g}{\delta^2\gamma_1^2\sigma r} \left(\frac{\sigma}{2} + \frac{b\rho\gamma_1^2}{4} \right),$$

the bifurcation is subcritical if

$$2\varepsilon\sqrt{r-1}\frac{|N_0|g}{\delta\gamma_1^2\sigma r} \left(\frac{\sigma}{2} + \frac{b}{4}\rho\gamma_1^2 \right) - (1+\sigma) > 0,$$

which requires $\varepsilon\delta > 0$. The condition can also be written

$$(1 + \sigma)(r - 1) - 2\sqrt{r - 1} \frac{|N_0|g}{|\delta|\gamma_1^2\sigma} \left(\frac{\sigma}{2} + \frac{b}{4}\rho\gamma_1^2 \right) \\ + 1 + \sigma < 0,$$

which means the bifurcation is subcritical for the corresponding h 's if r is between the two roots r_{\pm} of the following polynomial

$$(1 + \sigma)(\sqrt{r - 1})^2 - 2\sqrt{r - 1} \frac{|N_0|g}{|\delta|\gamma_1^2\sigma} \left(\frac{\sigma}{2} + \frac{b}{4}\rho\gamma_1^2 \right) \\ + 1 + \sigma = 0.$$

The value of r_{\pm} depends on the laser parameters. However, it can easily be shown that $1 < r_- \leq 2 \leq r_+$. The bifurcation is then never subcritical at threshold (i.e., at $h = h_c$), but may be subcritical for h 's very close to h_c . This fact strongly affects the validity range of the amplitude equations computed in the next paper.

4. Properties of traveling wave solutions

Above threshold, the amplitude of the electric field is given by

$$\bar{e}^2 = \frac{1}{2} \left(\frac{\delta_1}{b} - \delta_2 \right)^{-2} \\ \times \left[-2(\Omega - ah^2) \left(\frac{\delta_1}{b} - \delta_2 \right) - \frac{(1 + \sigma)^2}{b} + \sqrt{\mathcal{D}} \right]$$

where

$$\mathcal{D} = \left[2(\Omega - ah^2) \left(\frac{\delta_1}{b} - \delta_2 \right) + \frac{(1 + \sigma)^2}{b} \right]^2 \\ - 4 \left(\frac{\delta_1}{b} - \delta_2 \right)^2 [(\Omega - ah^2)^2 + (1 - r)(1 + \sigma)^2].$$

The value of h for which \bar{e}^2 is maximal is given by

$$\frac{d\bar{e}^2}{dh^2} = 0,$$

i.e.,

$$2a \left(\frac{\delta_1}{b} - \delta_2 \right) + \frac{1}{2\sqrt{\mathcal{D}}} \frac{d\mathcal{D}}{dh^2} = 0.$$

With

$$\frac{d\mathcal{D}}{dh^2} = -4a \left(\frac{\delta_1}{b} - \delta_2 \right) \frac{(1 + \sigma)^2}{b},$$

we get the equation for the curve on which laser emission is maximal:

$$1 = \frac{1}{\sqrt{\mathcal{D}}} \frac{(1 + \sigma)^2}{b},$$

i.e.,

$$\Omega - ah^2 = (\delta_1 - b\delta_2)(1 - r).$$

Finally, it is worth noting that when \bar{e}^2 is maximal, the electric field and the polarization are in phase. Indeed, with $\sqrt{\mathcal{D}} = \frac{(1 + \sigma)^2}{b}$, we get

$$\bar{e}^2 = \frac{1}{2} \left(\frac{\delta_1}{b} - \delta_2 \right)^{-2} \left[-2(\Omega - ah^2) \left(\frac{\delta_1}{b} - \delta_2 \right) \right] \\ = - \left(\frac{\delta_1}{b} - \delta_2 \right)^{-1} (\Omega - ah^2),$$

which reads

$$\alpha = \frac{1}{1 + \sigma} \left[\bar{e}^2 \left(\delta_2 - \frac{\delta_1}{b} \right) - (\Omega - ah^2) \right] = 0,$$

that is, $\bar{p} = \bar{e}$.

- [1] A.C. Newell, T. Passot, and J. Lega, *Annu. Rev. Fluid Mech.* **25**, 399 (1993).
- [2] M.C. Cross and P. C. Hohenberg, *Rev. Mod. Phys.* **65**, 851 (1993).
- [3] L.M. Narducci, J.R. Tredicce, L.A. Lugiato, N.B. Abraham, and D.K. Bandy, *Phys. Rev. A* **33**, 1842 (1986).
- [4] L.A. Lugiato, C. Oldano, and L.M. Narducci, *J. Opt. Soc. Am. B* **5**, 879 (1988).
- [5] L.A. Lugiato, G.-L. Oppo, M.A. Pernigo, J.R. Tredicce, L.M. Narducci, and D.K. Bandy, *Opt. Commun.* **68**, 63 (1988).
- [6] L.A. Lugiato, F. Prati, L.M. Narducci, P. Ru, J.R. Tredicce, and D.K. Bandy, *Phys. Rev. A* **37**, 3847 (1988).
- [7] P. Couillet, L. Gil, and F. Rocca, *Opt. Commun.* **73**, 403 (1989).
- [8] L.A. Lugiato, G.-L. Oppo, J.R. Tredicce, L.M. Narducci, and M.A. Pernigo, *J. Opt. Soc. Am. B* **7**, 1019 (1990).
- [9] H.G. Solari and R. Gilmore, *J. Opt. Soc. Am. B* **7**, 828

- (1990).
- [10] L. Gil, K. Emilson, and G.-L. Oppo, *Phys. Rev. A* **45**, 567 (1992).
- [11] P.K. Jakobsen, J.V. Moloney, A.C. Newell, and R. Indik, *Phys. Rev. A* **45**, 8129 (1992).
- [12] R. López Ruiz, G.B. Mindlin, C. Pérez-García, and J.R. Tredicce, *Phys. Rev. A* **47**, 500 (1993).
- [13] G.-L. Oppo, M. Brambilla, and L.A. Lugiato (unpublished).
- [14] W.J. Firth and E.M. Wright, *Opt. Commun.* **40**, 233 (1982).
- [15] W.J. Firth and E.M. Wright, *Phys. Lett.* **92A**, 211 (1982).
- [16] J.V. Moloney, *Opt. Acta* **29**, 1503 (1982).
- [17] J.V. Moloney and H.M. Gibbs, *Phys. Rev. Lett.* **48**, 1607 (1982).
- [18] J.V. Moloney, F.A. Hopf, and H.M. Gibbs, *Phys. Rev. A* **25**, 3442 (1982).

- [19] D.W. McLaughlin, J.V. Moloney, and A.C. Newell, *Phys. Rev. Lett.* **51**, 75 (1983).
- [20] J.V. Moloney, M. Sargent III, and H.M. Gibbs, *Opt. Comm.* **44**, 289 (1983).
- [21] J.V. Moloney, *J. Opt. Soc. Am.* **1**, 467 (1984).
- [22] J.V. Moloney, *Phys. Rev. Lett.* **53**, 556 (1984).
- [23] J.V. Moloney, *Philos. Trans. R. Soc. London Ser. A* **313**, 429 (1984).
- [24] D.W. McLaughlin, J.V. Moloney, and A.C. Newell, *Phys. Rev. Lett.* **54**, 681 (1985).
- [25] J.V. Moloney, *IEEE J. Quantum. Electron.* **QE-21**, 1393 (1985).
- [26] A. Aceves, H. Adachihara, C. Jones, J.C. Lehrmann, D.W. McLaughlin, J.V. Moloney, and A.C. Newell, *Physica D* **18**, 85 (1986).
- [27] J.V. Moloney, *Phys. Rev. A* **33**, 4061 (1986).
- [28] L.A. Lugiato and R. Lefever, *Phys. Rev. Lett.* **58**, 2209 (1987).
- [29] H. Adachihara, D.W. McLaughlin, J.V. Moloney, and A.C. Newell, *J. Math. Phys.* **29**, 63 (1988).
- [30] W.J. Firth, in *Instabilities and Chaos in Quantum Optics II*, edited by N.B. Abraham, F.T. Arecchi, and L.A. Lugiato (Plenum, New York, 1988), p. 219.
- [31] L.A. Lugiato and C. Oldano, *Phys. Rev. A* **37**, 3896 (1988).
- [32] A. Ouarzeddini, H. Adachihara, and J.V. Moloney, *Phys. Rev. A* **38**, 2005 (1988).
- [33] W.J. Firth and C. Paré, *Opt. Lett.* **13**, 1096 (1988).
- [34] G. Grynberg and J. Paye, *Europhys. Lett.* **8**, 29 (1989).
- [35] W.J. Firth, *J. Mod. Opt.* **37**, 151 (1990).
- [36] W.J. Firth, A. Fitzgerald, and C. Paré, *J. Opt. Soc. Am. B* **7**, 1087 (1990).
- [37] G.G. Luther and C.J. McKinstrie, *J. Opt. Soc. Am. B* **7**, 1125 (1990).
- [38] G. D'Alessandro and W.J. Firth, *Phys. Rev. Lett.* **66**, 2597 (1991).
- [39] G.G. Luther and C.J. McKinstrie, *J. Opt. Soc. Am. B* **9**, 1047 (1992).
- [40] R. Chang, W.J. Firth, R. Indik, J.V. Moloney, and E.M. Wright, *Opt. Commun.* **88**, 167 (1992).
- [41] G.S. McDonald and W.J. Firth, *J. Opt. Soc. Am. B* **10**, 1081 (1993).
- [42] A.L. Gaeta and R.W. Boyd, *Phys. Rev. A* **48**, 1610 (1993).
- [43] M. Saffman, D. Montgomery, A.A. Zozulya, K. Kuroda, and D.Z. Anderson, *Phys. Rev. A* **48**, 3209 (1993).
- [44] T. Honda (unpublished).
- [45] J.B. Geddes, R.A. Indik, J.V. Moloney, and W.J. Firth (unpublished).
- [46] C. Tamm, *Phys. Rev. A* **38**, 5960 (1988).
- [47] J.R. Tredicce, E.J. Quel, A. Ghazzawi, C. Green, M.A. Pernigo, L.M. Narducci, and L.A. Lugiato, *Phys. Rev. Lett.* **62**, 1274 (1989).
- [48] C. Green, G.B. Mindlin, E.J. D'Angelo, H.G. Solari, and J.R. Tredicce, *Phys. Rev. Lett.* **65**, 3124 (1990).
- [49] M. Brambilla, F. Battipede, L.A. Lugiato, V. Penna, F. Prati, C. Tamm, and C.O. Weiss, *Phys. A* **43**, 5090 (1991).
- [50] D. Dangoisse, D. Hennequin, C. Lepers, E. Louvergneaux, and P. Glorieux, *Phys. Rev. A* **46**, 5955 (1992).
- [51] E.J. D'Angelo, E. Izaguirre, G.B. Mindlin, G. Huyet, L. Gil, and J.R. Tredicce, *Phys. Rev. Lett.* **68**, 3702 (1992).
- [52] F.T. Arecchi, G. Giacomelli, P.L. Ramazza, and S. Residori, *Phys. Rev. Lett.* **67**, 3749 (1991).
- [53] J. Pender and L. Hesselink, *Opt. Lett.* **2**, 58 (1987).
- [54] J. Pender and L. Hesselink, *Opt. Lett.* **12**, 693 (1987).
- [55] G. Grynberg, E. Le Bihan, P. Verkerk, P. Simoneau, J.R.R. Leite, D. Bloch, S. Le Boiteux, and M. Ducloy, *Opt. Commun.* **67**, 363 (1988).
- [56] J. Pender and L. Hesselink, *IEEE J. Quantum Electron.* **25**, 395 (1989).
- [57] J. Pender and L. Hesselink, *J. Opt. Soc. Am. B* **7**, 1361 (1990).
- [58] D.J. Gauthier, M.S. Malcuit, A.L. Gaeta, and R.W. Boyd, *Phys. Rev. Lett.* **64**, 1721 (1990).
- [59] A. Petrossian, M. Pinard, A. Maître, J.-Y. Courtois, and G. Grynberg, *Europhys. Lett.* **18**, 689 (1992).
- [60] R. Macdonald and H.J. Eichler, *Opt. Commun.* **89**, 289 (1992).
- [61] R. Defreez, N. Yu, D.J. Bossert, M. Felisky, G.A. Wilson, R.A. Elliott, H.G. Winful, G.A. Evans, N.W. Carlson, and R. Amantea, *OSA Proceedings in Nonlinear Dynamics in Optical Systems*, edited by N.B. Abraham, E. Garmire, and P. Mandel [*Opt. Soc. Am.* **7**, 106 (1991)].
- [62] H. Haken, *Phys. Lett.* **53A**, 77 (1975).
- [63] A.C. Fowler, J.D. Gibbon, and M.J. McGuinness, *Physica* **4D**, 139 (1982).
- [64] R.G. Harrison, W. Lu, and P.K. Gupta, *Phys. Rev. Lett.* **63**, 1372 (1989).
- [65] W. Lu and R.G. Harrison, *Phys. Rev. A* **43**, 6358 (1991).
- [66] W. Eckhaus, *Studies in Nonlinear Stability* (Springer-Verlag, New York, 1965).
- [67] T.B. Benjamin and J.E. Feir, *J. Fluid Mech.* **27**, 417 (1967).
- [68] A.C. Newell, in *Lectures in Applied Mathematics, Nonlinear Wave Motion*, (American Mathematical Society, Providence, 1974), Vol. 15, pp. 157-163.
- [69] A.C. Newell and J.V. Moloney, *Nonlinear Optics* (Addison Wesley, Redwood City, CA, 1992).
- [70] L. Kramer and W. Zimmerman, *Physica D* **16**, 221 (1985).
- [71] L. Kramer, H. R. Schober, and W. Zimmerman, *Physica D* **31**, 212 (1988).
- [72] F.H. Busse, *Rep. Prog. Phys.* **41**, 1929 (1978).

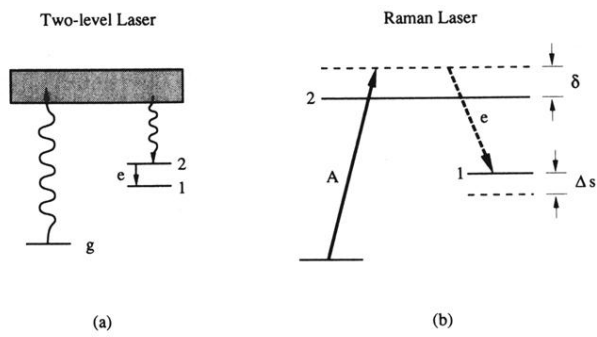
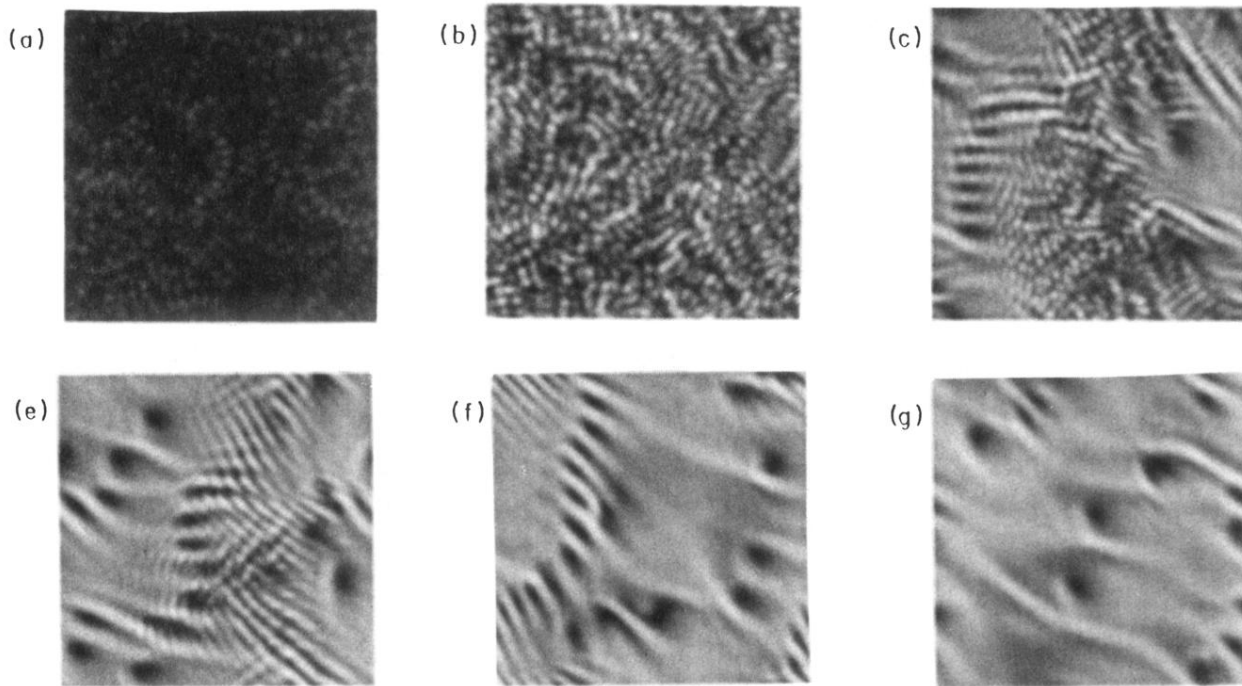


FIG. 1. Energy level diagrams depicting pumping schemes for a (a) two-level and (b) Raman laser.



NEAR-FIELD EMISSION

FIG. 10. Six frames from a movie showing the near-field (x, y) outputs of a Raman laser when the stress parameter $r = 3$. The other parameters are those of Fig. 8.

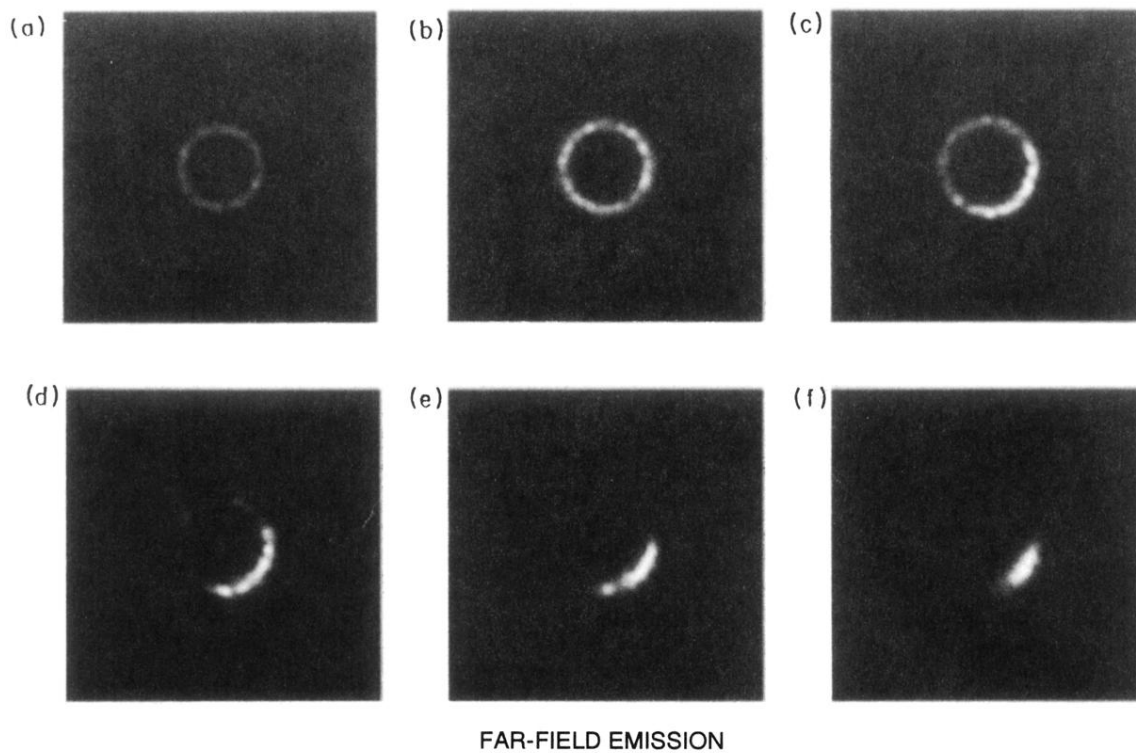
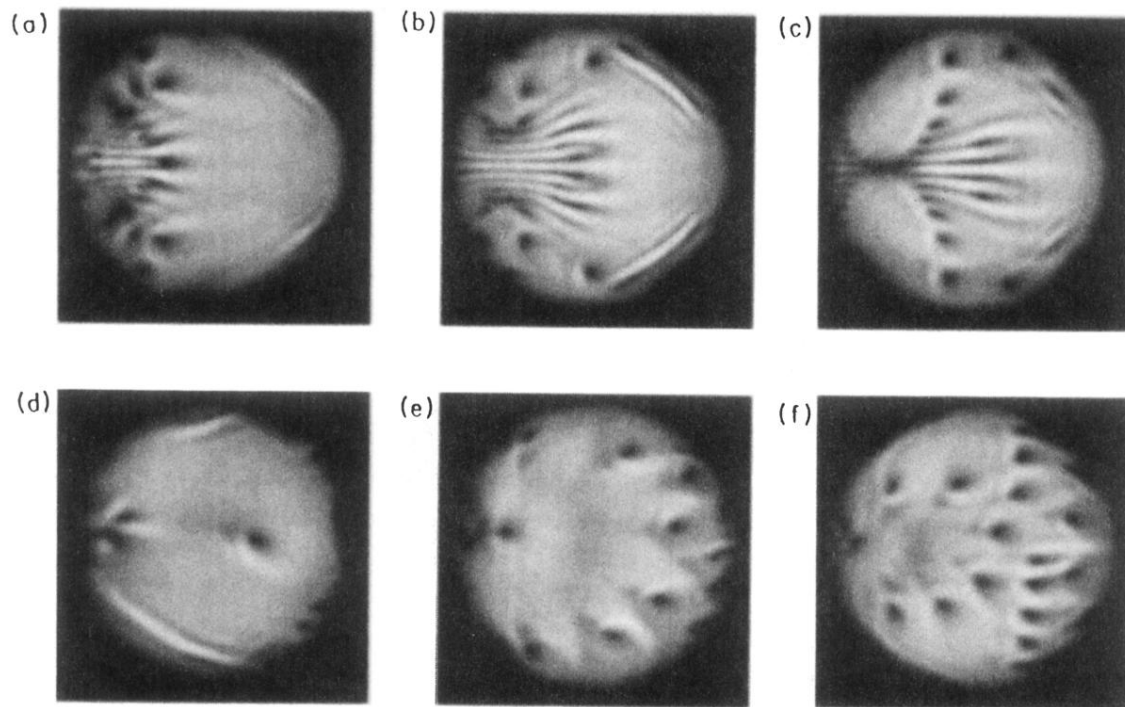


FIG. 11. Same as Fig. 10 for the corresponding far-field (k_x, k_y) outputs.



NEAR-FIELD EMISSION

FIG. 12. Near-field outputs of a Raman laser for a super-Gaussian pump, with an effective $r = 4$. The other parameters are those of Fig. 8.